Radiation Protection Dosimetry (2011), Vol. 143, No. 2–4, pp. 513–518 doi:10.1093/rpd/ncq513

MICRODOSIMETRIC COMPARISON OF SCANNED AND CONVENTIONAL PROTON BEAMS USED IN RADIATION THERAPY

John F. Dicello[1,*], Bradford B. Gersey[2], Daila S. Gridley[3], George B. Coutrakon[3,7], David Lesyna[4], Vincent L. Pisacane[5], James B. Robertson[6], Reinhard W. Schulte[3], Jerry D. Slater[3], Andrew J. Wroe[3] and James M. Slater[3]

[1]Department of Radiation Medicine, Loma Linda University Medical Center, 25 Westminster Bridge Way, Timonium, MD, USA
[2]NASA Center for Applied Radiation Research, Prairie View A&M University, S.R. Collins Rm. 111K, PO Box 519, Prairie View, TX 77446, USA
[3]Department of Radiation Medicine, Loma Linda University Medical Center, Chan Shun Pavillion, Room A-1010, 11175 Campus Street, Loma Linda, CA 92354, USA
[4]Optivus Proton Therapy, Inc, PO Box 608, Loma Linda, CA 92354, USA
[5]Aerospace Engineering Department (Mail Stop 11B), United States Naval Academy, 590 Holloway Road, Annapolis MD 21402–5042, USA
[6]East Carolina University, 408 Hillcrest Dr, Chocowinity, NC 27817, USA

*Corresponding author: dicello@usna.edu

Multiple groups have hypothesised that the use of scanning beams in proton therapy will reduce the neutron component of secondary radiation in comparison with conventional methods with a corresponding reduction in risks of radiation-induced cancers. Loma Linda University Medical Center (LLUMC) has had FDA marketing clearance for scanning beams since 1988 and an experimental scanning beam has been available at the LLUMC proton facility since 2001. The facility has a dedicated research room with a scanning beam and fast switching that allows its use during patient treatments. Dosimetric measurements and microdosimetric distributions for a scanned beam are presented and compared with beams produced with the conventional methods presently used in proton therapy.

INTRODUCTION

Fifty-five years ago, when the first clinical programmes of proton beam therapy began in the USA, Russia and Sweden, the hypothesis that better dose localisation and reduced doses to normal tissues would lead to better tumour control and less complications were not universally accepted. In the decades that followed, improved beam delivery and 3D localisation have emerged as major advances in radiotherapy. The first hospital-based proton treatment centre was opened at Loma Linda University Medical Center (LLUMC) in 1990. Clinical results of Phase I/II studies demonstrated high local tumour control rates in locally advanced base-of-skull, head-and-neck, oesophageal, lung, liver and prostate cancers with low late normal-tissue complications[1–4]. These results stimulated a surge of interest in the medical community, with of new proton centres the opening in USA and worldwide.

Recently, Hall[5] noted that 3D delivery techniques—in particular, intensity-modulated radiation therapy with photons (IMRT) and proton therapy—may expose patients to a larger dose of either leakage radiation from photon machines or neutrons in photon and proton therapy, with existing techniques potentially leading to a higher incidence of secondary tumours. He further suggested that the effective dose levels may be a significant function of the type of delivery with the benefits of protons only being achieved with scanning-beam techniques still under development at that time. Other investigators, in response to Dr Hall's papers, suggested that the levels of neutron dose associated with proton treatments could vary depending upon treatment techniques with estimates varying by factors of 10 or more from Hall's initial estimates[6–10].

Members of this group have been examining the dosimetric and biological consequences of doses outside of volumes treated with heavy charged-particle therapy beams for over 30 y[11, 12] At the James M. Slater, M.D. Proton Treatment and Research Center, the authors of this article have been carrying out preclinical and quality-assurance studies of proton beams used to treat patients. As part of those studies, researchers have examined the dosimetric, microdosimetric and biological properties inside and outside the treatment volumes[13–16]. The scanning proton beams discussed by Hall[5] had not yet been incorporated

[7]Present address: Department of Physics, Northern Illinois University, DeKalb, IL 60115, USA.

into the treatment delivery systems and were not readily available at that time. However, we had a scanning beam available at Loma Linda and have had the opportunity to examine the properties of this scanned beam for protons. It was the goal of this research to obtain preliminary measurements of (1) dose distributions outside treatment fields produced by passively modulated or actively scanned proton beams, and (2) doses and microdosimetric spectra both normal to, and downstream from, such treatment volumes.

METHODS AND RESULTS

Absorbed dose measurements for passively modulated and actively scanned proton beams

This section discusses techniques used to measure doses inside and outside proton fields for passively scattered and actively scanned proton beams at LLUMC then used for microdosimetric measurements. An experimental scanning beam has been available at the LLUMC proton facility since 2001, and LLUMC has FDA approval for its clinical application. LLUMC has a unique advantage in that it has a dedicated research room that can be utilised to produce a scanning beam for research with beam available, not only at night and on weekends, but also during patient treatments. With a very fast switching system, beam is available whenever beam is not actually being delivered to a patient. The dosimetry measurements reported here and the microdosimetry data presented below were obtained with the scanning beam in this Research Facility, in part, during patient treatment times.

The unmodulated initial proton beam was monoenergetic with an initial energy of 250 MeV, corresponding to a range in unit-density water of $\sim$37 cm. For both scenarios, 10×10 cm^2 and 14×14 cm^2 beams were incident on a phantom consisting of polystyrene blocks having lateral dimensions of 25×25 cm and 48-cm deep, sufficient to stop 250-MeV protons. Because of page limitations, data only for the larger field are presented in this paper.

Central-axis dose measurements for passively scattered and actively scanned beam delivery systems

The LLUMC proton facility uses a synchrotron accelerator with a nominal spill duration of 130 ms and a repetition rate of 0.45 Hz. For the measurements of passively scattered beams, one of the clinical beam lines at LLUMC was used. In the passive beam delivery system, called a nozzle, the beam is spread laterally to a maximum circular field of 20-cm diameter at isocentre using two scattering foils: one consisting of $\sim$0.5 cm of lead (Pb) and the other consisting of a contoured plastic disc of polycarbonate and lead (Pb) of comparable thickness. With this additional material in the beam line, the residual range for the 250-MeV proton beam was $\sim$27 cm. To achieve uniform dose coverage of the target volume throughout its depth, a rotating polycarbonate wheel of varying thickness intercepted the beam $\sim$1 m upstream of the phantom and attenuated the protons by various amounts to generate a spread out Bragg peak (SOBP) also called a modulated beam. The residual range of the modulated beam after being spread was $\sim$27 cm.

For the dose measurements using the passive-beam configuration to produce a treatment volume of $14\times14\times14$ cm^3, the dose was measured by placing a 0.6-cm diameter Marcus parallel-plate ionisation chamber in a phantom with the centre of range modulation at isocentre. The chamber had been cross-calibrated with an ion chamber recently calibrated at an ADCL laboratory using cobalt-60. The proton dose measurement was performed using the ICRU 59 protocol for clinical proton beams. In this way, the ionisation in the primary dose monitoring chamber of the nozzle could be calibrated in counts/Gy. When the microdosemeter was placed outside the field for the duration of the exposure, the proton dose to the target was absolutely calibrated to the nozzle's ionisation chamber response.

The set of measurements for the scanning beam used a monoenergetic 250 MeV raster-scanned spot beam in the research room to generate a 10×10 cm^2 and a 14×14 cm^2 field. Two scanning magnets were used to sweep the beam in both lateral dimensions. The scanning pattern was controlled by commanding a saw tooth waveform with 135 Hz frequency in one dimension and 5 Hz frequency in the other. The spill duration was increased to 370 ms for these measurements. Film exposures were made near the Bragg peak depth at 30 cm in polystyrene to determine that the dose uniformity was within ±5 % over the entire field when several hundred scans of the 14×14 cm^2 field were made. These lateral dose profiles are shown in Figure 1. The penumbra of the beam was typically $\sim$1 cm from 80 to 20 % of D_{max} at the lateral edges. The dose measurements were performed at 1-cm depth in polystyrene and at D_{max} as before. The nozzle transmission ionisation chamber was calibrated to the peak proton dose. The peak to entrance dose was also measured with the Marcus ion chamber and found to be $\sim$2.7.

Dose measurements outside the treatment field

For these sets of measurements, a large parallel plate ion chamber was placed beside the 25×25 cm^2 polystyrene blocks with the chamber's front surface at a distance of 5.5 cm from the edge of the field and abutting the phantom (i.e. 12.5 cm from the beam axis to the front of the chamber). The clinical beam line produced a passively scattered proton field of

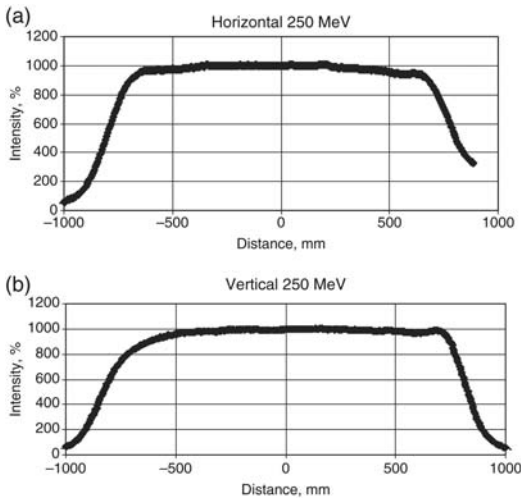

Figure 1. Dose profiles for a raster-scanned field, 14×14 cm, in the plane perpendicular to a horizontal 250-MeV proton beam.

14×14 cm^2 with 14 cm modulation in depth. As before, the composite thickness of the blocks was 48 cm, more than enough to stop the beam with a penetration depth of ~27 cm after passing through the two scattering foils. The active chamber volume was 15 cm in diameter with a 0.4-cm air gap. Measurements were taken at three positions (depths)—near the entrance region, in the Bragg-peak region, and downstream of the maximum range of the primary protons—and are listed in Tables 1 and 2. Using a known mass of the air and the charge collected from the ion chamber during the exposure, the dose outside the field could be calculated. The results are shown in Table 1.

For the set of measurements made adjacent to the 14×14 cm^2 field using a scanned 250-MeV beam, a chamber with a large sensitive volume was chosen because of the low dose rates; therefore, the doses reported are charge-integrated over a large collection volume with a reduced spatial resolution. The doses outside the field for the scanned beam were higher in comparison with the passively modulated beam, as shown in Table 2, and outside the estimated relative uncertainty of about ±10 %, noting that these doses are not point measurements but rather the integration over the entire volume of the chamber.

Table 1. Doses measured with a thickness of 12.5 cm of polystyrene from the central axis of the passively collimated beam to the surface of the parallel plate ionisation chamber, corresponding to 5.5 cm of absorber from the edge of the 14×14 cm^2 collimator.

Distance to central axis of chamber	Percentage of dose outside to central-axis dose
12.1 cm	0.57 %
24.25 cm	0.51 %
36 cm	0.12 %

Table 2. Doses measured at a distance of 12.5 cm from the central axis of the monoenergetic scanned beam for the specified amount of absorber upstream of the position where equivalent positions are at slightly different distances because of the different delivery systems.

Distance to central axis of chamber	Percentage of dose outside to central-axis dose
12.1 cm	0.74 %
26.0 cm	0.74 %
37.7 cm	0.70 %

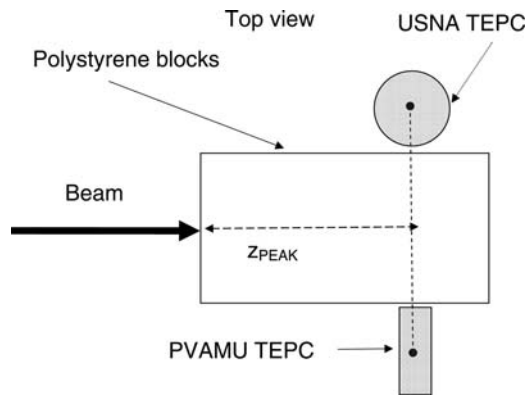

Figure 2. Typical setup for microdosimetric measurements with scanning, passively collimated or modulated beam incident on a polystyrene phantom of approximately unit density with two detectors positioned on opposing sides of phantom.

Microdosimetric distributions

A low average dose rate was initially anticipated for the scanning beam because it was still under development at the time of these measurements. For that reason, a HAWK spherical tissue-equivalent proportional counter, from the US Naval Academy and built by Far West Technology (USNA TEPC), with a 12.7-cm diameter sensitive volume and a right-circular cylindrical detector, with a sensitive volume of 1.75-cm diameter and axial length, provided by one of our coauthors, Bradford Gersey, from Prairie View A&M (PVAMU TEPC) were chosen. (In fact, the maximum dose rates were in excess of those needed for these studies.) The spherical detector was operated at a pressure to simulate a diameter of 2 μm in unit-density tissue and the cylindrical detector was operated to simualate 1-μm diameter and axial.

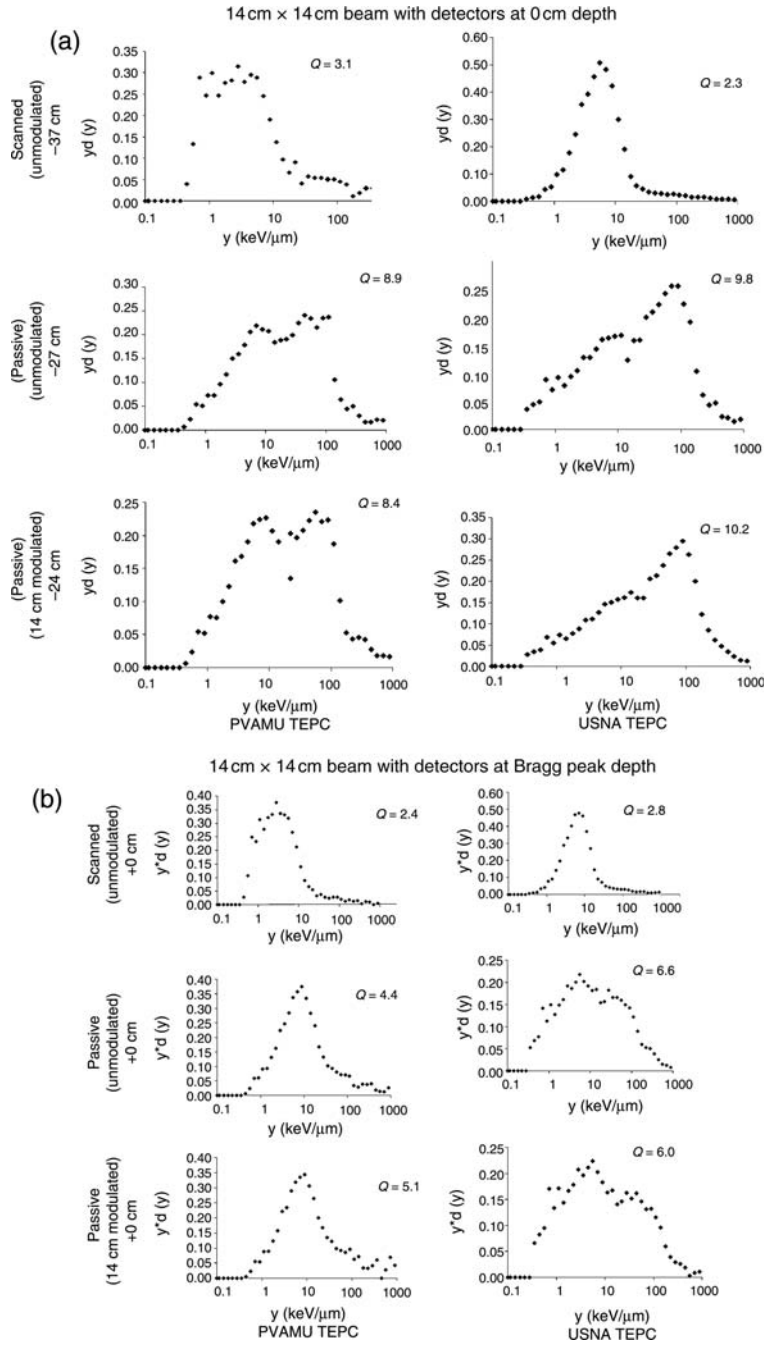

Figure 3. Microdosimetric spectra obtained with the two TEPCs described in text with simulated dimensions also given in the text at three positions as noted with the edge of the detectors abutting the phantom material at 12.5 cm lateral from central axis of beam. The detectors were positioned along the edges of a rectangular phantom with 12.5 cm of polystyrene from the central axis of the beams to the front of the detector. The mean Q Values calculated from the spectra are shown for each distribution for relative comparisons only; the Q values are not meant to represent expected tissue responses. (**a**) Detectors displaced 12.5 cm laterally at 0 cm downstream from front of phantom. (**b**) Detectors displaced 12.5 cm laterally at a depth corresponding to the Bragg-peak region. (**c**) Detectors displaced 12.5 cm laterally and at 48 cm from the front of phantom.

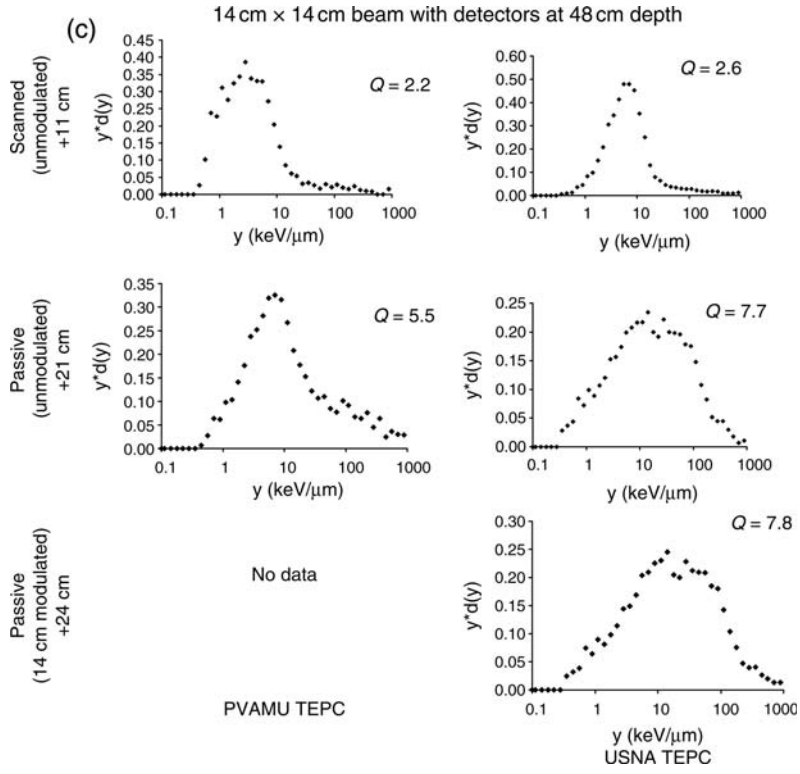

Figure 3. (Continued)

The positions of the chambers were selected to match those for the dose measurements and are demonstrated schematically in Figure 2 and listed in Figure 3 along with some of the data taken. Average quality factors, Q, are presented as a means of relative comparison only, and should not be interpreted as expected responses of either normal or malignant tissues. (The average quality factor is defined by the relation H=QD, where H is the dose equivalent and D is the physical absorbed dose; therefore, Q is the regulatory equivalent of the relative biological effectiveness of the radiation.)

DISCUSSION

Previous dosimetric and microdosimetric characterisations of the conventional proton therapy beams presently in use at Loma Linda conducted for two decades represented an important requirement for clinical utilisation of those beams. The present data represent the first microdosimetric study of scanned beams. The primary purpose of these measurements was to provide preliminary data for the design and execution of more comprehensive research studies. Nevertheless, these initial results provide an insight into many of the issues raised concerning proton therapy fields produced with scanned versus conventional methods. Spectra for the scanned beam show lower contributions from high-lineal energy events in both types of detectors relative to the passive beams, indicating a lower contribution from secondary neutrons as postulated by others previously. Both scanned and passive beams have major contributions from high-energy protons in the vicinity of 1–10 keV/μm, but the passive beams show more contributions from lower-energy protons, i.e. higher lineal energies up to ~100 keV/μm, perhaps the result of energy degradation although modulation does not appear to increase these events markedly. The contributions from events >100 keV/μm are not large, but that may be in part because these events may require lengthier exposure times to accumulate statistically observable numbers. Interestingly, the scanned beam shows higher physical doses relative to the central-axis doses than the passively collimated beams; so an assumption that scanned beams *a priori* have a lower effective dose would appear not to be justified. The largest Q values are immediately downstream of the collimator, but there are no large changes with increasing depth further downstream. The spectra for the scanned beam show differences in the distributions for the two types of detectors, suggesting significant displacement

factors and volume effects associated with the different types of chambers, and differences in response, although the mean Q values calculated from the spectra appear less sensitive. An important conclusion is that the dose rates even relatively far from the treatment volume are sufficiently large that smaller dosemeters and microdosemeters could be practically used in many cases, reducing volumetric or displacement artefacts.

REFERENCES

1. Bonnet, R. B. *et al. Effects of proton and combined proton/photon beam radiation on pulmonary function in patients with resectable but medically inoperable non-small cell lung cancer.* Chest. **120**, 1803–1810 (2001).
2. Hug, E. B. and Slater, J. D. *Proton radiation therapy for chordomas and chondrosarcomas of the skull base.* Neurosurg. Clin. N. Am. **11**, 627–638 (2000).
3. Slater, J. D. *et al. Proton therapy for prostate cancer: the initial Loma Linda University experience.* Int. J. Radiat. Oncol. Biol. Phys. **59**, 348–352 (2004).
4. Sugahara, S. *et al. Clinical results of proton beam therapy for cancer of the esophagus.* Int. J. Radiat. Oncol. Biol. Phys. **61**, 76–84 (2006).
5. Hall, E. J. *Intensity-modulated radiation therapy, protons, and the risk of second cancers.* Int. J. Radiat. Oncol. Biol. Phys. **65**, 1–7 (2006).
6. Hall, E. J. *The impact of protons on the incidence of second malignancies in radiotherapy.* Technol. Cancer Res. Treat. **6**, 31–34 (2007).
7. Gottschalk, B. *Neutron dose in scattered and scanned proton beams: in regard to Eric J. Hall (Int J Radiat Oncol Biol Phys 2006;65:1–7).* Int. J. Radiat. Oncol. Biol. Phys. **66**, 1594 (2006).
8. Macklis, R. *In regards to Hall: intensity-modulated radiation therapy, protons, and the risk of second cancers.* Int. J. Radiat. Oncol. Biol. Phys. **66**, 1593–1594 (2006) (Int J Radiat Oncol Biol Phys 2006;65:1–7).
9. Paganetti, H., Bortfeld, T. and Delaney, T. F. *Neutron dose in proton radiation therapy: in regard to Eric J. Hall (Int J Radiat Oncol Biol Phys 2006;65:1–7).* Int. J. Radiat. Oncol. Biol. Phys. **66**, 1594–1595 (2006).
10. Schneider, U. *et al. The impact of IMRT and proton radiotherapy on secondary cancer incidence.* Strahlenther Onkol. **182**, 647–652 (2006).
11. Amols, H. I., Bradbury, J. N., Dicello, J. F., Helland, J. F., Kligerman, M. M., Lane, T. G., Paciotti, M. A., Roeder, D. L. and Schillaci, M. E. *Dose outside the treatment volume for irradiation with negative pions.* Phys. Med. Biol. **23**, 385–396 (1978).
12. Amols, H. I., Dicello, J. F. and Zaider, M. *The RBE at various positions in and near a large negative pion beam.* In: Proceedings of the 6th Symposium on Microdosimetry. EURATOM EUR 6064 DE-EN-FR, pp. 433–440 (1978).
13. Robertson, J. B., Eaddy, J. M., Archambeau, J. O., Coutrakon, G. B., Miller, D. W., Moyers, M. F., Siebers, J. V., Slater, J. M. and Dicello, J. F. *Relative biological effectiveness and microdosimetry of a mixed energy field of protons up to 200 MeV.* Adv. Space Res. **14**, 271–275 (1994).
14. Wroe, A., Rosenfeld, A. and Schulte, R. *Out-of-field dose equivalents delivered by proton therapy of prostate cancer.* Med. Phys. **34**, 3449–3456 (2007).
15. Wroe, A., Clasie, B., Kooy, H., Flanz, J., Schulte, R. and Rosenfeld, A. *Out-of-field dose equivalents delivered by passively scattered therapeutic proton beams for clinically relevant field configurations.* Int. J. Radiat. Oncol. Biol. Phys. **73**, 306–313 (2009).
16. Clasie, B., Wroe, A., Kooy, K., Depauw, N., Flanz, J., Paganetti, H. and Rosenfeld, A. *Assessment of out-of-field absorbed dose and equivalent dose in proton fields.* Med. Phys. **37**, 311–321 (2010).